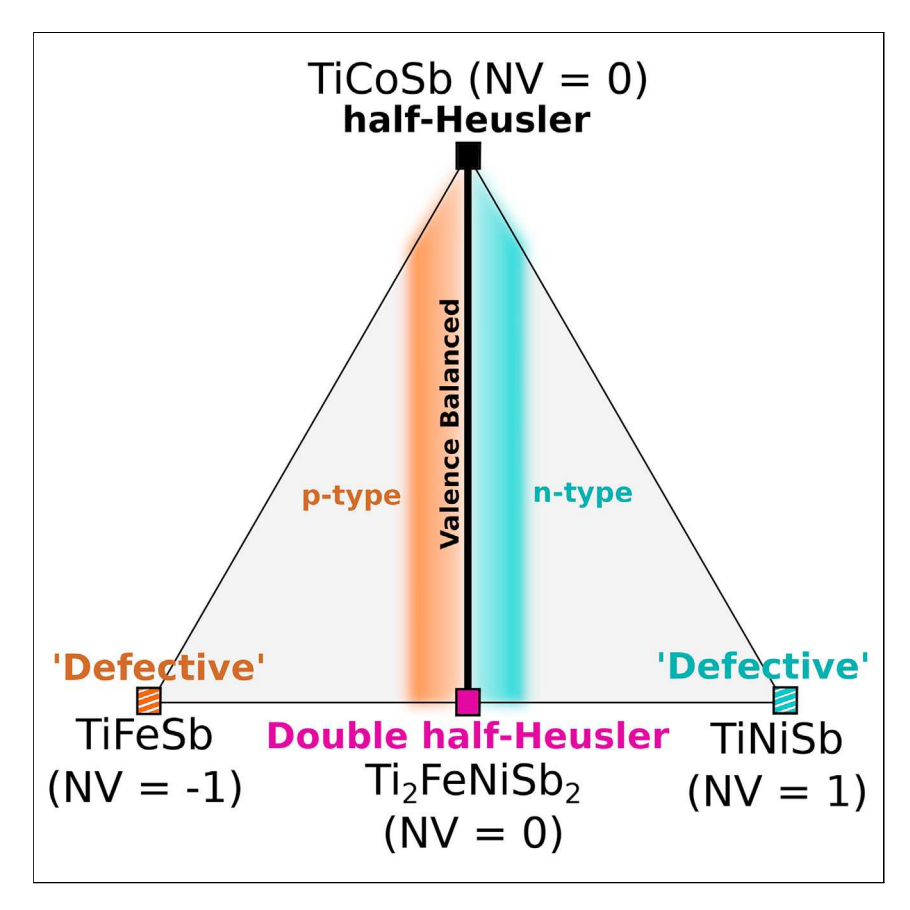


Report

Double Half-Heuslers



Despite decades of research on half-Heusler thermoelectrics, they are predominantly investigated as ternary compounds. From the same chemical phase space, we explore an enormous class of double half-Heuslers based on aliovalent substitution with ordered ground states. These compounds are constrained via crystal chemistry to exhibit much lower thermal conductivities (κ_L) relative to the well-known ternary compounds. Additional avenues for κ_L reduction via alloying with their "defective" ternary components emerge that significantly advance the search for high-performance thermoelectric half-Heuslers.

Shashwat Anand, Max Wood, Yi Xia, Chris Wolverton, G. Jeffrey Snyder

jeff.snyder@northwestern.edu

HIGHLIGHTS

Explore a vast class of double, triple, and quadruple half-Heusler semiconductors.

Demonstrated significantly low thermal conductivity in double half-Heuslers.

Demonstrated a simple strategy to discover multi-component intermetallic compounds.

Anand et al., Joule 3, 1–13 May 15, 2019 © 2019 Published by Elsevier Inc. https://doi.org/10.1016/j.joule.2019.04.003



Report

Double Half-Heuslers

Shashwat Anand, 1 Max Wood, 1 Yi Xia, 1 Chris Wolverton, 1 and G. Jeffrey Snyder 1,2,*

SUMMARY

Since their discovery around a century ago, multi-functional half-Heusler semiconductors have been studied extensively as three-component systems (nominal formula XYZ) with valence balanced compositions. From the very same set of elements and stability rules, we explore a much larger phase space of possible quaternary double $(X'X''Y_2Z_2, X_2Y'Y''Z_2, \text{ and } X_2Y_2Z'Z'')$, triple $(X_2'X''Y_3Z_3)$, and quadruple $(X_3'X''Y_4Z_4)$ half-Heusler compounds. Using reliable, first-principles thermodynamics on a selection (365) of previously unexplored compositions, we predict more quaternary compounds (131) than those predicted or reported extensively for the ternary systems (84). In comparison to state-of-the-art ternary half-Heusler thermoelectrics, for which performance is limited by their intrinsically high thermal conductivity (κ) , κ in double half-Heuslers is dominated by smaller group velocity phonons and limited by disorder scattering. The double half-Heusler $Ti_2FeNiSb_2$ was synthesized and confirmed to have a significantly lower κ than TiCoSb, thereby providing a better starting point for thermoelectric efficiency optimization.

INTRODUCTION

Half-Heusler compounds have attracted significant research attention for their thermoelectric properties ^{1–3} in the past decade. Due to its diverse chemical space to tune properties, multiple instances of high-performance thermoelectrics (NbFeSb, ⁴ TaFeSb, ⁵ and ZrCoBi ⁶ for p-type and TiNiSn^{7,8} for n-type transport) are found within this family of compounds. The high performance in half-Heusler compounds is primarily associated with their exceptional electrical transport properties. ⁹ However, in comparison to some of the best themoelectric materials based on IV-VI compounds, ^{10,11} ternary half-Heusler compounds are at a disadvantage due to their intrinsically large lattice thermal conductivity (κ_L). ZrCoBi, for example, ⁶ has one of the lowest reported κ_L of 10 W/(m.K) among the high-performing half-Heusler compounds (T = 300 K), whereas the state-of-the-art thermeoelectric material PbTe has intrinsic κ_L of 2 W/(m.K). ¹² Thus, it is desirable to find a strategy for discovering new semiconductors with the electronic properties of half-Heusler compounds but with inherently lower κ_L .

In addition to the well-known dependence of κ_L on chemical composition through phonon scattering ^{13,14} and lattice softening mechanisms, ^{6,14} κ_L also depends on the primitive unit cell size. ¹⁵ For two materials with comparable bulk properties, such as Debye temperature, average mass per unit cell, specific heat capacity, and Grüneisen parameter, the magnitude of κ_L depends primarily on the number of atoms in the primitive unit cell (N). ¹⁵ Complex materials with larger N have smaller κ_L due to a relatively small fraction of high group velocity (v_g) acoustic modes compared to lower v_g optical modes. Well-known examples of low κ_L materials with a large N are La₂Mo₂O₉ (N = 624, κ_L = 0.7 W/(m.K). ¹⁶ and Yb₁₄AlSb₁₁ (N = 104, κ_L = 0.6 W/(m.K). ^{15,17} For ternary half-Heuslers, however, N = 3, indicating the huge potential for low-thermal-conductivity materials discovery if the effective N could be increased systematically.

Context & Scale

Ternary half-Heusler compounds exhibit a fertile transition metal chemistry with properties relevant for themoelectrics, spintronics, topological band structures, and transparent conducting thin-film applications. For thermoelectric applications in particular, half-Heusler compounds are regularly reported with high thermoelectric power factors. However, thermoelectric efficiency in half-Heuslers suffers from intrinsically high thermal conductivities. Here, we explore a vast class of relatively unexplored double half-Heusler compounds that are constrained by crystal chemistry to exhibit much lower lattice thermal conductivities. Hence, we demonstrate a dependable strategy to assist the search for low-thermal-conductivity half-Heuslers and point toward a huge composition space for implementing it. Our findings can be extended for systematic discovery of other large families of multi-functional intermetallic semiconductors.



A well-known example of a family of compounds with varying cell sizes is based on the perovskite structure. ¹⁸ The high symmetry structures of the ternary perovskites (ABO_3 ; for example, cubic $BaTiO_3$) have N=5, while quaternary double perovskites ($A_2B'B''O_6$; for example, cubic Sr_2FeMoO_6 [N=10], monoclinic $La_2CuSnO_6^{19}$ [N=40]) have $N\geq 10$ when ordered. Double perovskites have a number of advantages over simple perovskites in tuning their functionalities for solar cell applications, magnetoresistive properties, etc. ^{18,20–22} With the additional possibilities of a new element, the number of double perovskites is also several times larger than simple perovskite compounds. ^{18,20}

Like perovskites, half-Heuslers can be made from a variety of elements, with each site occupied by elements in different regions of the periodic table (see Figure 1A). The possible ternary half-Heusler compositions (nominally XYZ) based on these elements can be chosen by assigning a valence to each element in the compound and imposing the valence balanced rule (a generalization of the well-known 18 electron rule for half-Heuslers), 25 according to which the net valence (NV) of the three components adds up to 0 for most stable compounds; e.g., NV of TiCoSb = 4 $(Ti^{+4} s^0 d^0) - 1 (Co^{-1} d^{10}) - 3 (Sb^{-3} s^2 p^6) = 0$. While quaternary compositions of the half-Heusler phases are studied routinely, these are almost always based on isovalent substitution between ternary systems with no unique valence balanced composition (for example, Ti_{0.5}Zr_{0.5}NiSn and Ti_{0.2}Zr_{0.8}NiSn) and hence do not favor the formation of ordered compounds like the double perovskites.²⁶ As a result, these alloy compositions often form disordered solutions, which are stabilized by temperature. Aliovalent substitution, however, can give rise to a unique valence balanced composition (for example, Fe and Ni substitution on the atomic Y-site in Ti₂FeNiSb₂; see Figure 1C), which is also characteristic of the compound forming 18-electron ternary half-Heuslers.²⁵ Hence, just like ternary half-Heuslers,²⁷ one can expect ordered ground states at these unique compositions to form stable compounds. Inspired by double perovskites, in which the "double" could refer to doubling of the perovskite formula unit $(A_2B'B''O_6)$ versus ABO_3 , we define double half-Heuslers (see Figure 1C) as stable quaternary compounds based on aliovalent substitution ($X_2Y'Y''Z_2$ versus XYZ, where Y' and Y" are not isovalent). To distinguish these compounds from the other isovalently alloyed quaternary compositions (for example, Ti_{0.5}Zr_{0.5}NiSn), we call these aliovalently substituted compounds (for example, Ti₂FeNiSb₂) double half-Heuslers, regardless of whether they undergo an order-disorder transition at a higher temperature. Although the disordered phase may have a distinct and possibly stronger scattering mechanism for phonons, the double half-Heusler composition ensures that for κ_L the effective N > 3.

The quaternary compositions of the double half-Heusler systems could present a much larger phase space for materials discovery in comparison to the ternary compositions. As we demonstrate here, there are a very large number of predicted stable double half-Heuslers awaiting experimental discovery. In addition to their applications as thermoelectrics, double half-Heuslers could also find use in transparent conducting thin films (e.g., $TalrGe^{28}$), topological semi-metals (e.g., $HflrAs^{27}$), and spintronics (e.g., $V_{0.8+\delta}CoSb^{24,29}$), for which the ternary half-Heuslers are already being studied.³⁰

RESULTS AND DISCUSSION

Locating Double Half-Heuslers in a Pseudoternary Phase Space

Consider the example of the pseudoternary $TiFe_xCo_yNi_{1-x-y}Sb$ (see Figure 1C), which allows for the aliovalent substitution of Fe, Co, and Ni atoms on the atomic

¹Department of Materials Science and Engineering, Northwestern University, Evanston, IL 60208, USA

²Lead Contact

^{*}Correspondence: jeff.snyder@northwestern.edu https://doi.org/10.1016/j.joule.2019.04.003



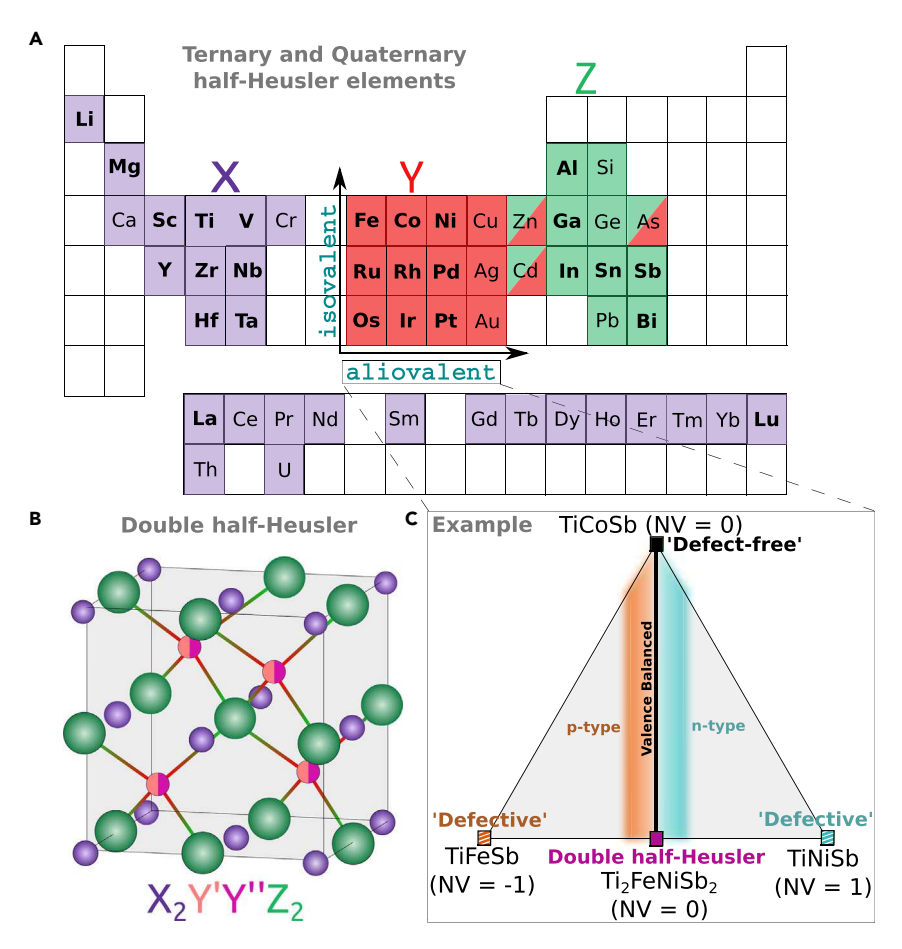


Figure 1. Visual Illustration of the Concept of Double Half-Heuslers

(A) Color scheme in the periodic table representing elements occupying various sites (X, violet; Y, red; Z, green) of the cubic half-Heusler structure (in B). Quaternary half-Heusler compositions selected in the present work are based on elements given in bold font.

(B) The double half-Heusler structure (disordered) with the general formula $X_2Y'Y'Z_2$ has equal occupancy on the Y-site (in half orange/half magenta) such that the overall composition is valence balanced (net valence NV = 0).

(C) Example pseudoternary $TiFe_xCo_yNi_{1-x-y}Sb$ based on aliovalent substitution on the atomic Y-site. Double half-Heusler $Ti_2FeNiSb_2$ (magenta square) and the alloy compositions joining it to TiCoSb (blue square) are valence balanced (NV=0). Adjacent compositions based on Fe (orange) and Ni (cyan) substitutions represent p and p-type compositions, respectively. Nominally $NV \neq 0$ ternary compositions (striped squares) are examples of defective half-Heuslers, which are unstable without defects ($TiFe_{1.5}Sb^{23}$ and $Ti_{0.75+a}NiSb^{24}$). These $NV \neq 0$ compositions will be referred to as the ternary components of the double half-Heusler composition.

Y-site (see Figure 1A). The end-members, namely TiFeSb, TiCoSb, and TiNiSb, all have different net valence (NV = -1, 0, and 1). In such a compositional phase space, the valence balanced end-members (like TiCoSb in Figure 1C) are candidates to form half-Heusler phases and have been studied rigorously (see Figure 2) either as experimental reports^{3,5,27,31} or as first-principles thermodynamic predictions. ^{3,5,27,31,32} Systems of the non-valence balanced end-members (TiFeSb and TiNiSb in Figure 1C), on the other hand, were not expected to form in the Heusler phase due to a perceived electronic configuration unfavorable for strong bonding interactions. ³⁰ However, the two NV \neq 0 systems shown (Ti-Fe-Sb and Ti-Ni-Sb) were recently reported to form half-Heusler phases at alternate defective stoichiometries (TiFe_{1.5}Sb and Ti_{0.75+8}NiSb, respectively) to attain a more stable

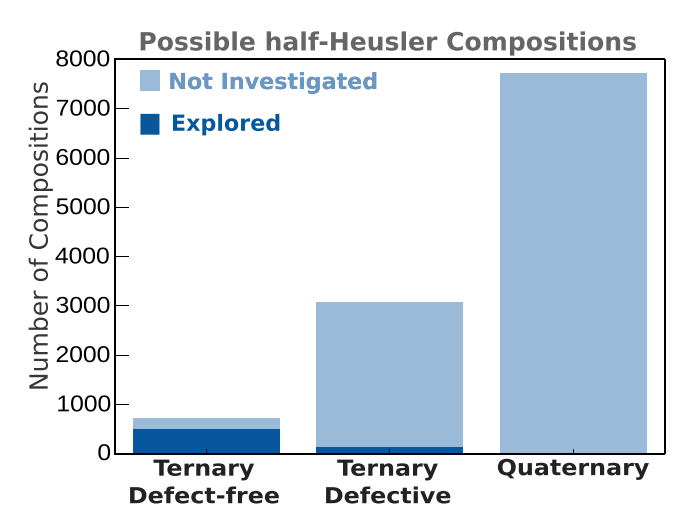


Figure 2. Number of Possible Ternary and Quaternary Half-Heusler Compositions

Bar chart depicting the current status of exploration in possible ternary half-Heusler systems as opposed to quaternary systems. The numbers of possible defect-free and quaternary compositions were obtained by imposing the valence balanced rule on the elemental combinations provided in Figure 1A. The remaining ternary combinations were classified as possible ternary defective compositions. The dark blue color gives a conservative estimate of the fraction of explored compositions. The quaternary phase space is almost completely unexplored.

electronic configuration. ^{23–25} Since these discoveries, nominally NV \neq 0 compounds have attracted some attention as ternary defective half-Heuslers (see Figures 1C and 2; K. Xia, P. Nan, Y. Wang, B. Ge, S.A., X. Zhao, G.J.S., and T. Zhu, unpublished data). ^{24,25,33,34} Possibly due to only one "likely" (NV = 0) half-Heusler candidate among the three end-members of such pseudoternaries, a large compositional space in the middle has seldom been investigated previously. However, the "double" half-Heusler composition, such as Ti₂FeNiSb₂ (4 [Ti⁺⁴ s⁰d⁰] – 1 [0.5 Fe⁻² d¹⁰] – 0 [0.5 Ni⁰ d¹⁰] – 3 [Sb⁻³ s²p⁶] = 0), and the alloy compositions connecting it to TiCoSb are also valence balanced with semiconducting *p*- and *n*-type transport achievable at adjacent compositions (see Figures 1C and S1). In the present work, we will refer to the nominally NV \neq 0 systems such as TiNiSb and TiFeSb as the two ternary components of the *quaternary double* half-Heusler compound, Ti₂FeNiSb₂.

Enormous Compositional Phase Space of *Quaternary Double*, *Triple*, and *Quadruple* Half-Heuslers

Similar to $Ti_2FeNiSb_2$, possible double half-Heusler compositions based on equal occupancies on the X- (e.g., $ScVCo_2Sb_2$) and Z-site (e.g., Ti_2Ni_2InSb) are also possible. Furthermore, there are additional "triple" (e.g., $Nb_2MgCo_3Sb_3$) and "quadruple" (e.g., $Nb_3LiCo_4Sb_4$) half-Heusler compositions as well, which obey the valence balanced rule (NV = 0). Applying the valence balanced rule to elemental combinations from Figure 1A (see Experimental Procedures), we find a huge phase space of 7,719 possible quaternary half-Heusler compositions (see Figure 2). This number is over 10 times larger than that of the defect-free ternary systems (715 possible compositions) based on the same set of elements. We estimate that the fraction of explored compositions (see Experimental Procedures) for defect-free ternary systems is $\sim 64\%$ (see Figure 2). In stark contrast, only 0.07% of the possible quaternary half-Heusler compositions have been explored, with 4 reports ($Ti_2FeNiSb_2$, 35 ScNbNi $_2Sn_2$, Zr_2Ni_2InSb , and Hf_2Ni_2InSb) of the half-Heusler phase in past experiments. There are no past reports—measurements or calculations—of thermal conductivity on such quaternary compositions in the literature.



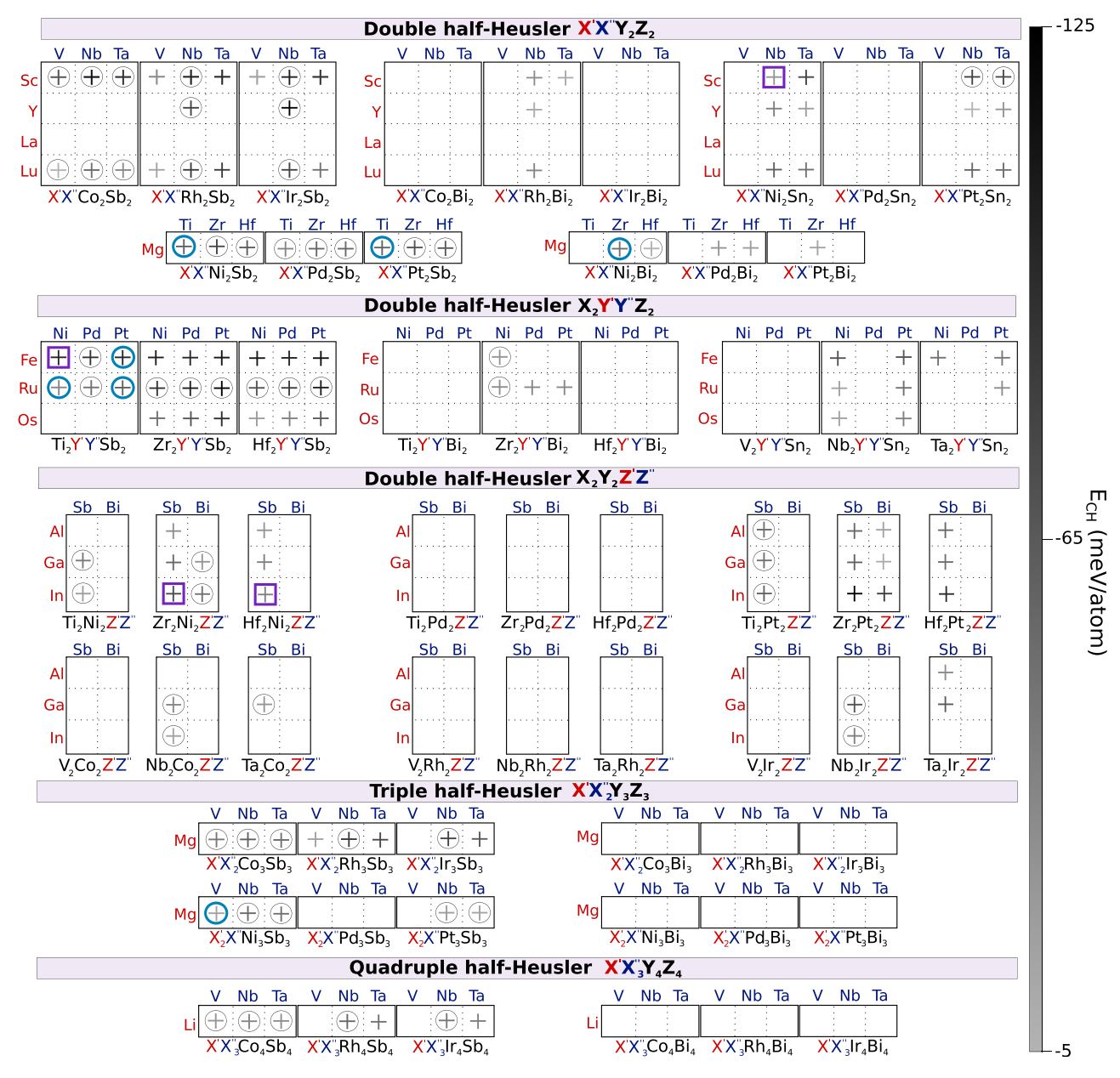


Figure 3. Predicted Quaternary Half-Heuslers and Stability

351 quaternary half-Heusler compositions (divided between 5 sub-types) investigated in the present work for stability in the half-Heusler structure. Half-Heuslers predicted stable are represented by a plus (+) symbol. For compounds where the half-Heusler phase is predicted unstable, the space is left blank. The grayscale bar on the side gives the magnitude of predicted stability (E_{CH} , see Table S1) of the quaternary half-Heuslers. Predicted compounds for which only one of the ternary NV \neq 0 components has a half-Heusler phase reported experimentally are denoted by thin circles (see Table S2). Predicted compounds for which both the ternary NV \neq 0 components have a half-Heusler phase reported experimentally are denoted by thick circles. Previously reported quaternary half-Heuslers are denoted by boxes.

Stability Prediction for Selected Double, Triple, and Quadruple Half-Heuslers

We select 369 quaternary half-Heusler (315 double half-Heusler, 36 *triple* half-Heusler, and 18 *quadruple* half-Heusler) compositions to perform high-throughput calculations for examining the thermodynamic stability using convex-hull analysis (see Figure 3) within the Open Quantum Materials Database (OQMD).^{37,38} In the present work, we avoid Ge-, As-, Pb-, and Si-based compounds, which have



relatively fewer reports of ternary half-Heuslers.^{27,31} The chosen compositions (given in Figure 3) are based on a subset of elements (given in bold font in Figure 1A) well known to commonly form ternary half-Heusler compounds.

The 315 double half-Heusler compositions studied here are divided into three classes (126 $X'X''Y_2Z_2$, 81 $X_2Y'Y''Z_2$, and 108 $X_2Y_2Z'Z''$ compositions) based on the site of substitution in the XYZ structure (see Figure 1A). Our calculations are in agreement with past experimental reports of the half-Heusler phase in Ti₂FeNiSb₂, 35 ScNbNi₂Sn₂, Zr₂Ni₂InSb, and Hf₂Ni₂InSb. ³⁶ We predict 48 X'X"Y₂Z₂, 36 X₂Y'Y"Z₂, and 27 $X_2Y_2Z'Z''$ new double half-Heusler compounds (see plus symbols in Figure 3), suggesting that substitution on either of the three atomic sites is quite favorable. Out of the 54 possible triple half-Heusler ($X_2'X''Y_3Z_3$) and quadruple half-Heusler $(X_3'X''Y_4Z_4)$ compositions combined, we predict 13 and 7 new compounds, respectively, of each sub-type (see Figure 3). Similar to ternary half-Heusler compounds, Sb-based compositions have the largest fraction of predicted stable compounds, followed by Sn- and then Bi-based compounds. This trend in stability of the semiconducting half-Heusler phases can be associated with the requirement of large size³¹ and large electronegativity for the Z-site atom. Although we do not calculate Asand Ge-based double half-Heuslers here, based on stability calculations and reports (see Table S4) of ternary half-Heuslers, we expect them to be relatively rarer.

Guidelines for Laboratory Discovery

Going through the list of 131 predicted new compounds using experimental synthesis can be quite daunting. To guide experimental efforts in initial choice of more likely compositions for laboratory discovery, we arrange (see color bar in Figure 3) the compounds according to their predicted stability determined by distance to the convex hull (E_{CH}). Compounds represented with darker plus symbols in Figure 3 are predicted to be more stable relative to decomposition into competing phases. The E_{CH} , formation energy (E_{form}), and band gap of the compounds predicted to be stable are given in Table S1 in descending order of predicted stability (E_{CH}).

We also use past experimental reports of the half-Heusler phase in ternary systems to categorize the predicted quaternary half-Heuslers by their likelihood to form compounds. The predicted quaternary half-Heuslers are based on aliovalent substitution in two nominally NV \neq 0 ternary XYZ structures (for example, TiFeSb and TiNiSb for Ti₂FeNiSb₂; see Figure 1C). As a result, the stability of quaternary half-Heuslers must be correlated to the stability of their ternary NV \neq 0 components, which are investigated to a relatively larger extent (see ternary defective bar in Figure 2). Based on this rationale, the likelihood of predicted quaternary half-Heusler phase stabilizing increases depending on whether one (see thin circles in Figure 3; for example, Ti₂Ni₂InSb) or both (see thick circles in Figure 3; for example, MgTiNi₂Sb₂) of its ternary NV \neq 0 components have a half-Heusler phase previously reported for them. We caution that this classification based on past experimental reports may not be complete simply because a large fraction of ternary nominally NV \neq 0 systems are still unexplored (see Figure 2 and Table S2).

Valence Balanced Rule as a Dependable Strategy for Discovery of Low κ_L Quaternary Half-Heuslers

We compare measured κ_L of double half-Heusler Ti₂FeNiSb₂ to that of its corresponding ternary system TiCoSb with the same average atomic mass. At room temperature, κ_L of Ti₂FeNiSb₂ is smaller than TiCoSb by a factor of 3 (see Figure 4A). To examine the origin of the smaller κ_L in Ti₂FeNiSb₂, we calculate the κ_L of its ordered ground state from first principles considering only three-phonon processes (see



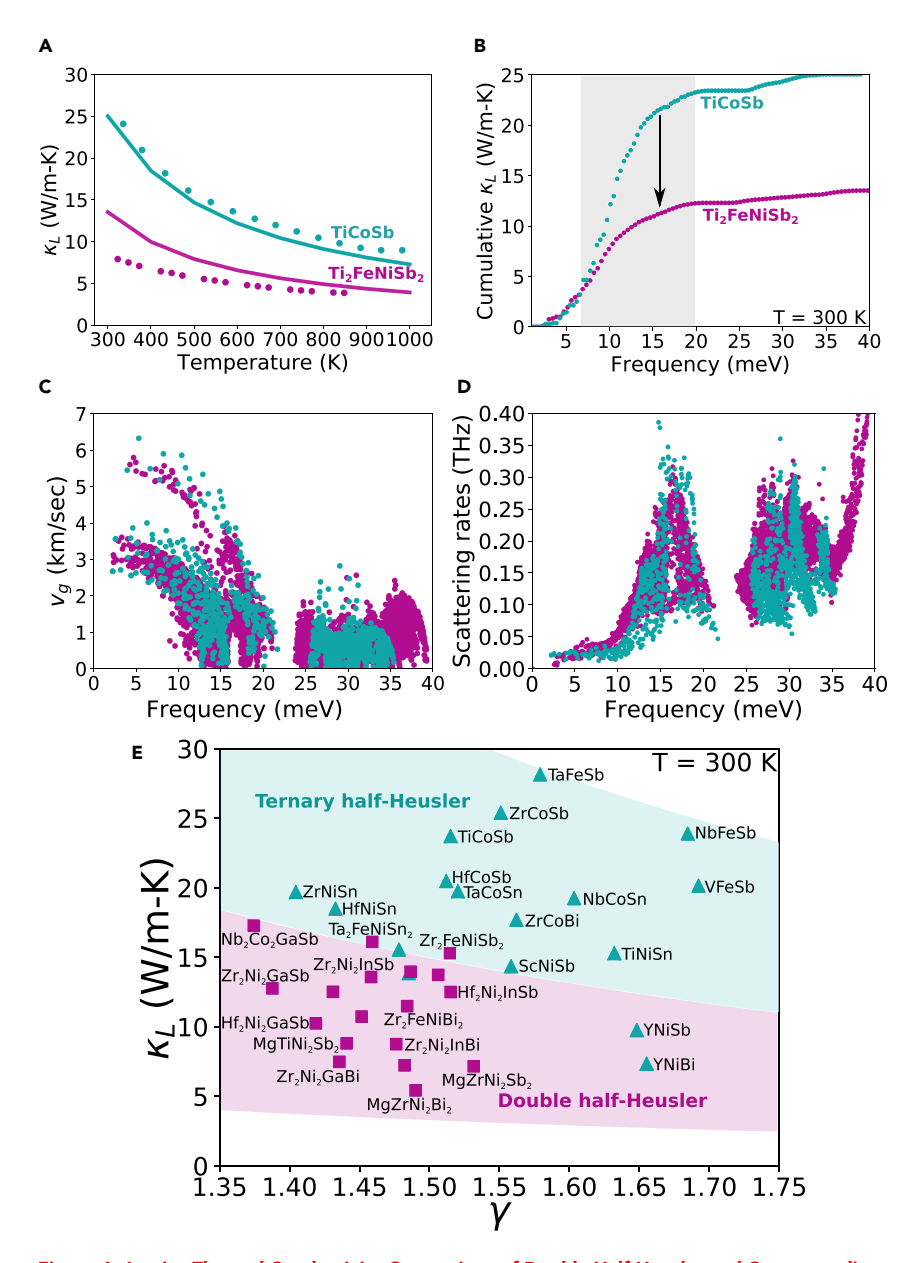


Figure 4. Lattice Thermal Conductivity Comparison of Double Half-Heusler and Corresponding Ternary Half-Heusler

(A) Calculated (line) and measured (scatter points) lattice thermal conductivity (κ_L) of TiCoSb (cyan) and Ti₂FeNiSb₂ (magenta) as a function of temperature. Experimental values of TiCoSb are taken from Sekimoto et al. ³⁹

(B–D) Calculated phonon frequency dependence of (B) cumulative κ_L , (C) group velocities (v_g), and (D) phonon-phonon scattering rates in the two compounds at T=300 K.

(E) Calculated κ_L versus Grüneisen parameter (γ) for selected half-Heusler (triangle) and double half-Heusler (square) compounds based on commonly used elements (see Table S3). The regions are shaded based on a γ^{-2} dependence of κ_L .

Figure 4A). The calculated κ_L is very similar to the measured values, especially at higher temperatures.

Calculated cumulative κ_L in TiCoSb and Ti₂FeNiSb₂ as a function of frequency (see Figure 4B) suggests that over 90% of the thermal transport in both compounds occurs in





phonon modes corresponding to the acoustic modes of the ternary structure. The difference in the κ_L between the two compounds occurs primarily in the high energy range (7–20 meV, see shaded gray region in Figure 4B) corresponding to the acoustic modes of TiCoSb. Both compounds largely show a similar dependence of group velocity (v_a) as well as scattering rates on phonon frequencies (see Figure 4). However, the v_q of phonons in Ti₂FeNiSb₂ is in general much lower than that of the corresponding longitudinal and transverse acoustic modes of TiCoSb (see Figure 4C). As can been understood from simple ball-spring models for cell doubling, 15 the difference in v_q becomes more prominent in the higher frequency range (10-20 meV) of the acoustic modes in TiCoSb (see Figure 4C). The phonon scattering rates of the double half-Heusler Ti₂FeNiSb₂ structure are also slightly larger in the 7-12 meV frequency range (see Figure 4D). The trend of lower κ_1 for double half-Heuslers compared to ternary half-Heuslers is reproduced in a survey of 35 compounds (see Figure 4E and Table S3) calculated in a similar way. This confirms our expectation that double half-Heusler with the more complex crystal chemistry would in general have lower lattice thermal conductivities than traditional ternary half-Heusler.

The weaker temperature dependence in the measured κ_L of Ti₂FeNiSb₂ in comparison to the calculated values (see Figure 4A) can possibly be attributed to the presence of alloy scattering mechanism associated with disorder in the Fe/Ni sub-lattice. The disorder in the system was confirmed by the powder XRD pattern of Ti₂FeNiSb₂ (see Figure S2) as no superlattice peaks associated with Fe/Ni ordering were observed. The alloy scattering mechanism is not captured in our κ_L calculations, which were performed on the ordered Ti₂FeNiSb₂ structure assuming only Umklapp scattering, which has a relatively stronger (T^{-1}) temperature dependence when compared to the alloy scattering mechanism.

To understand the observed global cubic symmetry of the half-Heusler phase, we estimate the energy difference between the ordered and disordered phase by calculating the energy of the special quasi-random structure of Ti₂FeNiSb₂. The disordered phase of Ti₂FeNiSb₂ is only 23.6 meV/mixing atom higher in energy than the ordered phase. This difference in energy can be overcome by thermal energy alone at 275 K, thereby explaining the observed disordered Ti₂FeNiSb₂ phase. Recent reports of short-range ordering observed in electron diffraction pattern of ternary defective half-Heuslers suggests that short-range ordering (K. Xia, P. Nan, Y. Wang, B. Ge, S.A., X. Zhao, G.J.S., and T. Zhu, unpublished data) could also exist in double half-Heusler compounds, and its impact on thermal conductivity should also be considered. It is important to note that double half-Heuslers could be alloyed with the defective half-Heusler phases $(Ti_{0.75+\delta}NiSb^{24,25}$ and $TiFe_{1.5}Sb^{23})$ of its ternary components to introduce vacancies and interstitial defects, which can be expected to decrease the thermal conductivity further. While the alloy scattering mechanisms of phonons are good for thermoelectric applications by reducing thermal conductivity, the same scattering mechanisms are also likely to reduce charge carrier mobility and electrical conductivity, possibly depending on site of substitution.⁴⁰ The net benefit in thermoelectric performance would be characterized by the ratio of κ_l to charge carrier mobility.⁴¹

Potential for Exploration of Low-Cost Thermoelectrics in Quaternary Half-Heusler Phase Space

While other quaternary compounds can be investigated for thermodynamic stability, the current prediction of 131 new compounds is already greater than the 84^{3,5,27,31,42} (see Table S4) extensively predicted or reported transition-metal-based ternary defect-free half-Heusler phases. This result suggests that, despite a hundred years of Heusler history, only a small fraction of half-Heuslers have been investigated previously. Among the new



compounds predicted here, 32 are based on relatively abundant or inexpensive elements (namely Li, Mg, Y, Ti, Zr, Hf, V, Nb, Ta, Fe, Ni, Co, Al, Ga, In, Sn, Sb, and Bi; see Table S1) commonly used for synthesis of half-Heusler compounds and serve as an immediate prediction for experimental synthesis. Given the intrinsically smaller κ_L of quaternary half-Heusler compounds (see Figure 4E) due to their complex crystal chemistry, they present a new avenue for thermoelectric materials discovery. The present work only deals with quaternary equivalents of transition-metal-based half-Heusler compounds with 18-valence electrons. The concepts discussed here are easily applicable to other multi-component Heusler-based structures, 43 such as 8-electron Nowotny-Juza phases (e.g., LiAlSi), 44,45 f-block element-based half-Heuslers (e.g., DyNiBi), 46 24-electron full-Heuslers (e.g., VFe₂Al), 30,47,48 and Li-based 18-electron Heuslers, 49 opening up the possibility for an even larger phase space of materials with versatile properties.

Conclusion

We demonstrate that the number of known half-Heusler-based semiconductors, despite their hundred years of history, may only be a fraction of the actual number of stable compounds. The previously unexplored semiconductor compositions can be conceived by choosing aliovalently substituted combinations, which are valence balanced and predicted systematically using first-principles thermodynamics of stability. From this strategy, we discover quaternary (double, *triple*, and *quadruple*) half-Heusler compounds with thermal conductivities intrinsically lower than traditional ternary half-Heuslers, owing to their complex crystal chemistry. As a result, we significantly advance the decade-long search for low-thermal-conductivity half-Heuslers without tampering with the underlying transition metal chemistry, which forms the basis of their exciting properties suitable for thermoelectrics, spintronics, topological band structures, and transparent conducting thin films.

EXPERIMENTAL PROCEDURES

Thermodynamic Stability Calculations

The density functional theory (DFT) calculations⁵⁰ in this study were performed using Vienna ab initio simulation package (VASP)⁵¹ to determine the lowest-energy ground state among the structural derivatives enumerated by the enumlib code. 52,53 We used Perdew-Burke-Ernzerhof (PBE) formulation of the exchange-correlation energy functional derived under a gradient-generalized approximation (GGA).⁵⁴ Plane-wave basis sets are truncated at an energy cutoff of 350 eV, and a Γ -centered k-point mesh with a density of \sim 8,000 k-points per reciprocal atom (KPPRA) was used. All structures were relaxed with respect to cell vectors and their internal degrees of freedom until forces on all atoms were less than 0.1 eV nm⁻¹ before calculating their formation enthalpies (E_{form}) . The Open Quantum Materials Database $(OQMD)^{37,38}$ was used to perform convex-hull analysis for examining thermodynamic stability against all other known phases in the respective composition space. The prototype of ordered structures used in the thermodynamic stability calculations are $Ti_2FeNiSb_2$ (N = 12, space group I-42d), $VScCo_2Sb_2$ (N = 12, space group $Pmn2_1$), Ti_2Ni_2InSb (N = 12, space group I-42d), MgTiNi₂Sb₂ (N = 12, space group I-42d), MgNb₂Co₃Sb₃ (N = 18, space group Cc), and LiNb₃Co₄Sb₄ (N = 12, space group I-42 m). Compounds based on small-sized elements (Ga and Al) are known to stabilize in the orthorhombic (space group Pnma) structure. 27,31 For such compounds, we tested stability of the half-Heusler structure against that of the orthorhombic structural derivatives.

Estimating Explored and Unexplored Composition Space of Possible Half-

To estimate the number of possible ternary (defect-free) and quaternary half-Heusler compositions (see Figure 2), we applied the valence balanced rule (NV = 0) on





various combinations based on the elements in Figure 1A. We used a valence of +1for Li, +2 for group-II elements, +3 for group-III elements and rare-earth Lanthanides, +4 for group-IV elements, Cr, and Actinides, -2 for group-VIII elements, -1 for group-IX elements, 0 for group-X elements, +1 for group-XI elements, +2 for group-XII elements, -5 for Al, Ga, and In, -4 for Si, Ge, Sn, and Pb, and -3 for As, Sb, and Bi. The number of ternary defective compositions were counted by the nominally NV \neq 0 combinations based on the elements in Figure 1A. To estimate the number of compositions explored previously, we counted all the cases contained in the inorganic crystal structure database (ICSD)⁴² and those examined through rigorous high-throughput computations.^{3,5,27,31} As these are "possible" half-Heusler compositions, we counted all compositions at which there is a predicted or reported compound, irrespective of whether it forms in the half-Heusler phase. Cases in which these compositions phase separate are documented systematically in a few computational reports and are also counted in our estimate of explored compositions. 3,5,27,31,32 Experimental cases of such negative results are typically not reported in the literature and are not contained in any databases such as the ICSD. Hence, our count of explored ternary and quaternary compositions can be considered as a conservative estimate of the explored phase space.

κ_L Calculations

 κ_L calculations were performed within the framework of anharmonic lattice dynamics and the Boltzmann transport equation, assuming that three-phonon interactions and isotope scattering dominate the total phonon scattering rates. To overcome the formidable computational cost in evaluating third-order interatomic force constants (IFCs), we employed the recently developed compressive sensing lattice dynamics (CSLD) method 55,56 to efficiently extract both harmonic and anharmonic IFCs, the accuracy of which is further verified by comparing to the third-order IFCs obtained by finite displacement method. 57,58 Afterward, ShengBTE package 58 was employed to numerically solve the Boltzmann transport equation (BTE) under relaxation time approximation (RTA). The convergence of the calculated κ_L was carefully examined with respect to the cutoff diameter of the third-order anharmonic IFCs and the grid of sampled phonon wavevector. We found that cutoff diameters of 5 and 4.5 Å were sufficient to yield κ_L with good convergence in half-Heusler and double half-Heusler, respectively.

Synthesis

The sample of $Ti_2FeNiSb_2$ was prepared using an arc melter using stoichiometric ratios of bulk Ti slugs (99.99% Sigma-Aldrich), Fe lumps (99.99% Alpha Aesar), Fe Ni slugs (99.99% Alpha Aesar), and Fe Sb shot (99.999% Alpha Aesar). Starting elements were cut into small pieces and loaded into an Edmund Büehler MAM-1 Arc Melter, where they were melted together Fe times, flipping in between each melt. The arc-melted button was then pulverized in a stainless steel vial for Fe 1 h using a SPEX Sample Prep 800 Series Mixer/Mill. This powder was consolidated using an induction-heated rapid hot press under a flowing argon atmosphere within a Fe 1/2-in-diameter high-density graphite die (POCO). This sample was then pressed at Fe 1,100°C for Fe 1 h at a pressure of 45 MPa. Once pressed, this sample was polished to remove excess graphite from its surface, sealed in an evacuated fused silica ampule, and annealed at 900°C for 1 week.

Characterization

Transmission XRD was performed on powder pulverized from the pellet using a STOE STADI-MP X-ray diffractometer using Cu K- α radiation. Electronic transport measurements were measured under dynamic high vacuum up to 875 K with a ramp speed of 75 K/h. Resistivity and Hall coefficient were measured concurrently using the van der



Pauw technique with pressure-assisted molybdenum contacts equipped a 2 T magnet. Thermal diffusivity measurements were taken with a Netzch LFA 457 under purged flowing argon up to 875 K with a ramp speed of 75 K/h. Thermal conductivity was calculated estimating heat capacity with the Dulong-Petit law. Seebeck coefficient was measured under dynamic high vacuum up to 875 K with a homebuilt system using Chromel-Nb thermocouples. κ_L was calculated by subtracting the electronic contribution from the calculated total thermal conductivity. The electronic portion of thermal conductivity was found using the Wiedemann-Franz law, in which a variable Lorenz number was used based on the sample's Seebeck coefficient.

SUPPLEMENTAL INFORMATION

Supplemental Information can be found online at https://doi.org/10.1016/j.joule. 2019.04.003.

ACKNOWLEDGMENTS

S.A. would like to thank Vinay Ishwar Hegde for fruitful discussion on the subject of thermodynamic phase stability and high-throughput calculations. G.J.S. and S.A. acknowledge support from the "Designing Materials to Revolutionize and Engineer our Future" program of the National Science Foundation under Award No. 1729487 and the U.S. Department of Energy, Office of Energy Efficiency and Renewable Energy (EERE). C.W. (DFT calculations) acknowledges support from the U.S. Department of Energy, Office of Science and Office of Basic Energy Sciences, under Award No. DE-SC0014520.

AUTHOR CONTRIBUTIONS

G.J.S. and S.A. conceived and designed the project; S.A. performed the thermodynamic stability and lattice thermal conductivity calculations; M.W. carried out the synthesis and characterization; Y.X. mentored high-throughput thermal conductivity calculations; S.A., Y.X. and G.J.S. analyzed thermal conductivity calculations; C.W. mentored the computational aspect of the project; G.J.S. mentored the experimental aspect of the project. S.A., M.W., C.W., and G.J.S. prepared and edited the manuscript.

DECLARATION OF INTERESTS

The authors declare no competing interests.

Received: February 9, 2019 Revised: March 17, 2019 Accepted: April 1, 2019 Published: April 9, 2019

REFERENCES

- Zeier, W.G., Schmitt, J., Hautier, G., Aydemir, U., Gibbs, Z.M., Felser, C., and Snyder, G.J. (2016). Engineering half-Heusler thermoelectric materials using Zintl chemistry. Nat. Rev. Mater. 1, 16032.
- Zhu, T., Liu, Y., Fu, C., Heremans, J.P., Snyder, J.G., and Zhao, X. (2017). Compromise and Synergy in high-efficiency thermoelectric materials. Adv. Mater. 29, 1605884.
- Mao, J., Liu, Z., Zhou, J., Zhu, H., Zhang, Q., Chen, G., and Ren, Z. (2018). Advances in thermoelectrics. Adv. Phys. 67, 69–147.
- Fu, C., Bai, S., Liu, Y., Tang, Y., Chen, L., Zhao, X., and Zhu, T. (2015). Realizing high figure of merit in heavy-band p-type half-Heusler thermoelectric materials. Nat. Commun. 6, 8144
- Zhu, H., Mao, J., Li, Y., Sun, J., Wang, Y., Zhu, Q., Li, G., Song, Q., Zhou, J., Fu, Y., et al. (2019). Discovery of TaFeSb-based half-Heuslers with high thermoelectric performance. Nat. Commun. 10, 270.
- 6. Zhu, H., He, R., Mao, J., Zhu, Q., Li, C., Sun, J., Ren, W., Wang, Y., Liu, Z., Tang, Z., et al. (2018).
- Discovery of ZrCoBi based half Heuslers with high thermoelectric conversion efficiency. Nat. Commun. 9, 2497.
- Sakurada, S., and Shutoh, N. (2005). Effect of Ti substitution on the thermoelectric properties of (Zr, Hf)NiSn half-Heusler compounds. Appl. Phys. Lett. 86, 082105.
- Rogl, G., Sauerschnig, P., Rykavets, Z., Romaka, V., Heinrich, P., Hinterleitner, B., Grytsiv, A., Bauer, E., and Rogl, P. (2017). (V, Nb)-doped half heusler alloys based on {Ti, Zr, Hf}NiSn with high zT. Acta Mater. 131, 336–348.



- Zhou, J., Zhu, H., Liu, T.-H., Song, Q., He, R., Mao, J., Liu, Z., Ren, W., Liao, B., Singh, D.J., et al. (2018). Large thermoelectric power factor from crystal symmetry-protected non-bonding orbital in half-Heuslers. Nat. Commun. 9, 1721.
- Pei, Y., Shi, X., LaLonde, A., Wang, H., Chen, L., and Snyder, G.J. (2011). Convergence of electronic bands for high performance bulk thermoelectrics. Nature 473, 66–69.
- Heremans, J.P., Jovovic, V., Toberer, E.S., Saramat, A., Kurosaki, K., Charoenphakdee, A., Yamanaka, S., and Snyder, G.J. (2008). Enhancement of thermoelectric efficiency in PbTe by distortion of the electronic density of states. Science 321, 554–557.
- Romero, A., Gross, E., Verstraete, M., and Hellman, O. (2015). Thermal conductivity in PbTe from first principles. Phys. Rev. B 91, 214310.
- Wood, M., Aydemir, U., Ohno, S., and Snyder, G.J. (2018). Observation of valence band crossing: the thermoelectric properties of CaZn₂Sb₂-CaMg₂Sb₂ solid solution. J. Mater. Chem. A Mater. Energy Sustain. 6, 9437–9444.
- 14. Tan, G., Hao, S., Hanus, R.C., Zhang, X., Anand, S., Bailey, T.P., Rettie, A.J., Su, X., Uher, C., Dravid, V.P., et al. (2018). High thermoelectric performance in SnTe–AgSbTe₂ alloys from lattice softening, giant phonon–vacancy scattering, and valence band convergence. ACS Energy Lett. 3, 705–712.
- Toberer, E.S., Zevalkink, A., and Snyder, G.J. (2011). Phonon engineering through crystal chemistry. J. Mater. Chem. 21, 15843–15852.
- Winter, M.R., and Clarke, D.R. (2007). Oxide materials with low thermal conductivity. J. Am. Ceram. Soc. 90, 533–540.
- Toberer, E.S., Cox, C.A., Brown, S.R., Ikeda, T., May, A.F., Kauzlarich, S.M., and Snyder, G.J. (2008). Traversing the metal-insulator transition in a zintl phase: rational enhancement of thermoelectric efficiency in Yb₁₄Mn_{1-x}Al_xSb₁₁. Adv. Funct. Mater. *18*, 2795–2800.
- Vasala, S., and Karppinen, M. (2015). A₂B'B"O₆ perovskites: a review. Prog. Solid State Chem. 43. 1–36.
- Anderson, M.T., and Poeppelmeier, K.R. (1991). Lanthanum copper tin oxide (La₂CuSnO₆): a new perovskite-related compound with an unusual arrangement of B cations. Chem. Mater. 3, 476–482.
- Kanhere, P., and Chen, Z. (2014). A review on visible light active perovskite-based photocatalysts. Molecules 19, 19995–20022.
- Kangsabanik, J., Sugathan, V., Yadav, A., Yella, A., and Alam, A. (2018). Double perovskites overtaking the single perovskites: A set of new solar harvesting materials with much higher stability and efficiency. Phys. Rev. Mater. 2, 055401.
- 22. Kobayashi, K.-I., Kimura, T., Sawada, H., Terakura, K., and Tokura, Y. (1998). Roomtemperature magnetoresistance in an oxide material with an ordered double-perovskite structure. Nature 395, 677–680.
- Naghibolashrafi, N., Keshavarz, S., Hegde, V.I., Gupta, A., Butler, W., Romero, J., Munira, K., LeClair, P., Mazumdar, D., Ma, J., et al. (2016).

- Synthesis and characterization of Fe-Ti-Sb intermetallic compounds: Discovery of a new Slater-Pauling phase. Phys. Rev. B 93, 104424.
- Anand, S., Xia, K., Zhu, T., Wolverton, C., and Snyder, G.J. (2018). Temperature dependent n-type self doping in nominally 19-electron half-heusler thermoelectric materials. Adv. Energy Mater. 8, 1801409.
- Anand, S., Xia, K., Hegde, V.I., Aydemir, U., Kocevski, V., Zhu, T., Wolverton, C., and Snyder, G.J. (2018). A valence balanced rule for discovery of 18-electron half-Heuslers with defects. Energy Environ. Sci. 11, 1480.
- Page, A., Van der Ven, A., Poudeu, P., and Uher, C. (2016). Origins of phase separation in thermoelectric (Ti, Zr, Hf)NiSn half-heusler alloys from first-principles. J. Mater. Chem. A Mater. Energy Sustain. 4, 13949–13956.
- Gautier, R., Zhang, X., Hu, L., Yu, L., Lin, Y., Sunde, T.O., Chon, D., Poeppelmeier, K.R., and Zunger, A. (2015). Prediction and accelerated laboratory discovery of previously unknown 18electron ABX compounds. Nat. Chem. 7, 209, 214.
- Yan, F., Zhang, X., Yu, Y.G., Yu, L., Nagaraja, A., Mason, T.O., and Zunger, A. (2015). Design and discovery of a novel half-Heusler transparent hole conductor made of all-metallic heavy elements. Nat. Commun. 6, 7308.
- Ma, J., Hegde, V.I., Munira, K., Xie, Y., Keshavarz, S., Mildebrath, D.T., Wolverton, C., Ghosh, A.W., and Butler, W. (2017). Computational investigation of half-heusler compounds for spintronics applications. Phys. Rev. B 95, 024411.
- Graf, T., Felser, C., and Parkin, S.S. (2011).
 Simple rules for the understanding of Heusler compounds. Prog. Solid State Chem. 39, 1–50.
- Zakutayev, A., Zhang, X., Nagaraja, A., Yu, L., Lany, S., Mason, T.O., Ginley, D.S., and Zunger, A. (2013). Theoretical prediction and experimental realization of new stable inorganic materials using the inverse design approach. J. Am. Chem. Soc. 135, 10048– 10054.
- Carrete, J., Li, W., Mingo, N., Wang, S., and Curtarolo, S. (2014). Finding unprecedentedly low-thermal-conductivity half-heusler semiconductors via high-throughput materials modeling. Phys. Rev. X 4, 011019.
- Zeier, W.G., Anand, S., Huang, L., He, R., Zhang, H., Ren, Z., Wolverton, C., and Snyder, G.J. (2017). Using the 18-electron rule to understand the nominal 19-electron halfheusler NbCoSb with Nb vacancies. Chem. Mater. 29, 1210–1217.
- Xia, K., Liu, Y., Anand, S., Snyder, G.J., Xin, J., Yu, J., Zhao, X., and Zhu, T. (2018). Enhanced thermoelectric performance in 18-electron Nb_{0.8}CoSb Half-Heusler compound with intrinsic Nb vacancies. Adv. Funct. Mater. 28, 1705845.
- Toboła, J., Jodin, L., Pecheur, P., Scherrer, H., Venturini, G., Malaman, B., and Kaprzyk, S. (2001). Composition-induced metalsemiconductor-metal crossover in half-heusler Fe_{1-x}Ni_xTiSb. Phys. Rev. B 64, 155103.

- Skolozdra, R., Romaka, L., Aksel'rud, L., Mel'nik, G., and Tatomir, Y.T. (1999). New phases of MgAgAs, LiGaGe and TiNiSi structural types containing d-and p-elements. Heopl'an. marep. 35, 456–460.
- Kirklin, S., Saal, J.E., Meredig, B., Thompson, A., Doak, J.W., Aykol, M., Rühl, S., and Wolverton, C.M. (2015). The Open Quantum Materials Database (OQMD): Assessing the accuracy of DFT formation energies. npj Comput. Mater. 1, 15010.
- Saal, J.E., Kirklin, S., Aykol, M., Meredig, B., and Wolverton, C. (2013). Materials design and discovery with high-throughput density functional theory: the open quantum materials database (OQMD). JOM 65, 1501– 1509.
- Sekimoto, T., Kurosaki, K., Muta, H., and Yamanaka, S. (2006). Thermoelectric and thermophysical properties of TiCoSb-ZrCoSb-HfCoSb pseudo ternary system prepared by spark plasma sintering. Mater. Trans. 47, 1445– 1448.
- Wang, H., Cao, X., Takagiwa, Y., and Snyder, G.J. (2015). Higher mobility in bulk semiconductors by separating the dopants from the charge-conducting band-a case study of thermoelectric pbse. Mater. Horiz. 2, 323–329.
- Wang, H., LaLonde, A.D., Pei, Y., and Snyder, G.J. (2013). The criteria for beneficial disorder in thermoelectric solid solutions. Adv. Funct. Mater. 23, 1586–1596.
- 42. Hellenbrandt, M. (2004). The inorganic crystal structure database (ICSD)—present and future. Crystallogr. Rev. 10, 17–22.
- Kim, K., Ward, L., He, J., Krishna, A., Agrawal, A., and Wolverton, C. (2018). Machinelearning-accelerated high-throughput materials screening: Discovery of novel quaternary heusler compounds. Phys. Rev. Mater. 2, 123801.
- Bockelmann, W., and Schuster, H.-U. (1974). Kristallchemische aspekte ternärer phasen des lithiums mit 3B-und 4B-elementen in elektrovalenter und nicht elektrovalenter zusammensetzung. Zeitschrift füranorganische und allgemeine Chemie 410, 241–250.
- Barth, J., Fecher, G.H., Schwind, M., Beleanu, A., Felser, C., Shkabko, A., Weidenkaff, A., Hanss, J., Reller, A., and Kohne, M. (2010). Investigation of the thermoelectric properties of LiAlSi and LiAlGe. J. Electron. Mater. 39, 1856–1860.
- Dwight, A.E. (1974). Crystal structure of DyNiSb, DyPtSb and related compounds. In: Proc. Rare Earth Res. Conf., 11th, Michigan, 2, 642
- Vasundhara, M., Srinivas, V., and Rao, V. (2005). Low-temperature electrical transport in heusler-type Fe₂V(AISi) alloys. J. Phys. Condens. Matter 17, 6025.
- He, J., Amsler, M., Xia, Y., Naghavi, S.S., Hegde, V.I., Hao, S., Goedecker, S., Ozolinš, V., and Wolverton, C. (2016). Ultralow thermal conductivity in full heusler semiconductors. Phys. Rev. Lett. 117, 046602.



- He, J., Naghavi, S.S., Hegde, V.I., Amsler, M., and Wolverton, C. (2018). Designing and discovering a new family of semiconducting quaternary heusler compounds based on the 18electron rule. Chem. Mater. 30, 4978–4985.
- Kohn, W., Becke, A.D., and Parr, R.G. (1996). Density functional theory of electronic structure. J. Phys. Chem. 100, 12974– 12980.
- Kresse, G., and Furthmüller, J. (1996).
 Efficient iterative schemes for ab initio totalenergy calculations using a plane-wave basis set. Phys. Rev. B Condens. Matter 54, 11169– 11186.
- 52. Hart, G.L., and Forcade, R.W. (2008). Algorithm for generating derivative structures. Phys. Rev. B 77, 224115.
- Hart, G.L., Nelson, L.J., and Forcade, R.W. (2012). Generating derivative structures at a fixed concentration. Comput. Mater. Sci. 59, 101–107.
- Perdew, J.P., Burke, K., and Ernzerhof, M. (1996). Generalized gradient approximation made simple. Phys. Rev. Lett. 77, 3865–3868.
- Zhou, F., Nielson, W., Xia, Y., and Ozolins, V. (2014). Lattice anharmonicity and thermal conductivity from compressive sensing of

- first-principles calculations. Phys. Rev. Lett. 113, 185501.
- Zhou, F., Nielson, W., Xia, Y., and Ozolins, V. (2018). Compressive sensing lattice dynamics. I. General formalism. arXiv, arXiv:1805.08904. https://arxiv.org/abs/1805.08904.
- Togo, A., and Tanaka, I. (2015). First principles phonon calculations in materials science. Scr. Mater. 108, 1–5.
- Li, W., Carrete, J., Katcho, N.A., and Mingo, N. (2014). ShengBTE: a solver of the Boltzmann transport equation for phonons. Comput. Phys. Commun. 185, 1747–1758.